https://cimav.repositorioinstitucional.mx/jspui/

Theoretical and experimental study of the photocatalytic activity of ZnO coated tubular reactor

E. Ríos-Valdovinos, P. Amézaga-Madrid, W. Antúnez-Flores, F. Pola-Albores, P. Pizá-Ruíz, M. Miki-Yoshida

Abstract

ZnO thin films were deposited inside of fused silica tubing by aerosol assisted chemical vapor deposition technique. The films were transparent, uniform, highly adherent and non-light scattering. Photocatalytic activity of internally ZnO coated tubing was evaluated by discoloration of a methyl orange aqueous solution in a batch reactor. Tubing was externally irradiated with UV-A at room temperature. A one dimensional model was proposed to calculate the spatial distribution of the carrier density and the films' surface charge carrier concentration. This model can explain the influence of the films thickness on the photocatalytic activity. Results showed that the photocatalytic activity largely depends on the film thickness. For external irradiation of the films the optimum thickness was around 60–70 nm, for which the photocatalytic activity was maximum. The photonic efficiency of internally ZnO coated tubular reactors was evaluated as a function of initial colorant concentration, irradiation time and intensity. Furthermore, due to the high activity of the ZnO films, the films were repeatedly exposed to UV-A irradiation cycles, followed by activity measurement.

Keywords: AACVD, ZnO coated tubing, Photocatalytic properties, Photonic efficiency, Carrier distribution model.

Introduction

The degradation of organic compounds based on heterogeneous photocatalysis of semiconductor oxides, has been extensively investigated as an alternative for an efficient control of environmental pollutants [1–4]. Among many semiconductors studied, TiO_2 has been known as the best photocatalyst due to several properties such as chemical stability, high photocatalytic activity and no toxicity [5–7]. In recent years, ZnO has attracted special attention in the degradation of environmental pollutants, mainly for various reasons such as physical stability, high oxidative capacity, low cost and similar band gap energy at room temperature (3.37 eV) as TiO_2. It can be activated by light from natural or artificial sources (fluorescent lamp) to generate electron and hole pairs (e^-, h^+) and later to interact with adsorbed species (OH^-, O_2) [8,9]. Generated electrons and holes can react independently with adsorbed species depending upon the exact conditions (photocatalyst, pH, redox potential of species). For example, electrons can reduce dioxygen to superoxide ion $O_2^{\bullet-}$; and holes can react with water to produce hydroxyl radical $OH^{\bullet}$. However, to maintain charge neutrality of the photocatalyst it is required that oxidative and reductive reactions take place simultaneously. Further studies have confirmed that ZnO is an environmentally friendly material and exhibits more efficiency than TiO_2 in photocatalytic decomposition of some organic compounds in aqueous solution [10,11]. In fact, it has been reported about the ZnO dissociation in aqueous solution to give Zinc ions. It is well known that zinc ions are toxic but different revisions about heterogeneous photocatalysis using ZnO as photocatalyst have reported that the solubility of ZnO is low and it only could be increased at particular

range of temperature and pH of the aqueous medium [12–15]. Zinc oxide may undergo acid, electrochemical corrosion and photocorrosion at pH values below 7 [16,17].

Most of photocatalytic studies of ZnO have been performed with powder suspensions. In spite of the high surface area of the powder particles and its high photocatalytic efficiency, exists two main drawbacks. Firstly, it takes place the turbidity of the aqueous medium created when the catalyst is in suspension, decreasing the amount of sunlight that interacts with the catalyst. Secondly, it is necessary a final separation steps to recovering and recycling the photocatalyst after completion of the degradation process [18,19]. Therefore, immobilization of the photocatalyst as a thin film on inert support, such as glass [20], ceramics [21], plastic fiber-optic cable [22] or glass fiber [23], eliminates the turbidity and the separation step of the photocatalyst, reducing process time and cost, so leading to a wider range of applications [24,25].

Thin films can be prepared by various techniques such as sol–gel [26], electron beam evaporation [27], RF magnetron sputtering [28], spray pyrolysis [29], pulsed laser deposition [30] and aerosol assisted CVD (AACVD) [31]. Among these techniques, AACVD provides more advantages in controlling the microstructure, composition and thickness of the films, and they could be obtained on flat or tubular substrates.

In this work, the photocatalytic activity of ZnO coated tubular reactors was evaluated by the photo-discoloration of a basic organic dye (methyl orange, MO). A one-dimensional model of the distribution of photogenerated carrier density and surface carrier concentration was calculated and used to explain the variation of reaction rate

with the thickness of the film. The variation of average photonic efficiency was evaluated as a function of MO concentration, irradiation time and irradiation intensity.

Materials and methods

Materials: Zinc acetate [$(CH_3CO_2)_2Zn$, Aldrich, 99.99%] was used in this work as chemical precursor. The solvent was absolute ethanol (C_2H_6O, J.T. Baker). Methyl orange, MO, ($C_{14}H_{14}N_3NaO_3S$, Sigma–Aldrich, 85%) was the model pollution for discoloration. All chemicals were analytical reagent grade and were used without further purification.

ZnO thin film-coated reactor preparation: ZnO thin films were synthesized inside fused silica tubing by AACVD technique. The overall dimensions of the tubing were inside diameter (ID) of 7 mm and length (L) of 230 mm. Details of the deposition system was reported previously [8]. The process started from aerosol generation of precursor solution in the nebulizer using a 0.1 M solution of zinc acetate in absolute ethanol. This aerosol was injected into the heated tubing inside the cylindrical furnace, using micro-filtered air as carrier gas at 310 kPa and 67 $cm^3\ s^{-1}$. Several deposition temperatures were tried between 250 and 500 °C. The deposition time was varied between 7.5 and 45 min in order to obtain different film thickness. Table 1 summarizes the principal preparation parameters used in this work. After deposition, all the samples were heat treated in air at 450 °C for 2 h to decompose possible organic residues deposited in the film surface and to stabilize the microstructure.

Microstructural characterization: Scanning electron microscopy (SEM) was used to establish the composition and surface morphology of the films. This examination was

realized in a field emission JSM-7401F scanning electron microscope, coupled with an Oxford Inca X-ray energy dispersive spectrometer (EDS).

In addition, UV–vis reflectance spectra were used for thickness determination. These spectra were obtained in an F-20 UV optical fiber reflectance spectrophotometer in contact probe mode. Samples were analyzed in many sections to verify the axially and azimuthally film thickness uniformity.

Photocatalytic activity measurements: Different aqueous solutions of analytic grade MO dye were prepared, with their concentrations ranging from 0.0076 to 0.31 mmol L^{-1}. Previous calibration curves of solution concentration vs. absorbance were obtained in a UV-VIS Lambda 10 spectrophotometer.

The photocatalytic activity of the samples was evaluated in terms of the photo-discoloration of MO under UV-A irradiation at room temperature. MO was used as the test contaminant, a dye extensively used as an indicator for the study of photocatalytic activities [32,33] exhibiting two absorption maxima: the first and most intense band is observed at around 460 nm, and the second and less intense at 270 nm. The measurements were carried out in a segment (7 cm) of ZnO coated tubing with a snap cap used as batch reactor. Internally film coated tubings were externally irradiated with a UV-A lamp (UVP model UVL-36), at adequate distance (1–2 cm) to obtain the desired irradiation. The film coated tubing was filled with 1.5–2.0 mL of the MO solution and it was exposed to the UV-A lamp. Fig. 1 illustrates the transversal cross section of the internally coated fused silica tubing (FS), used for the photocatalytic evaluation.

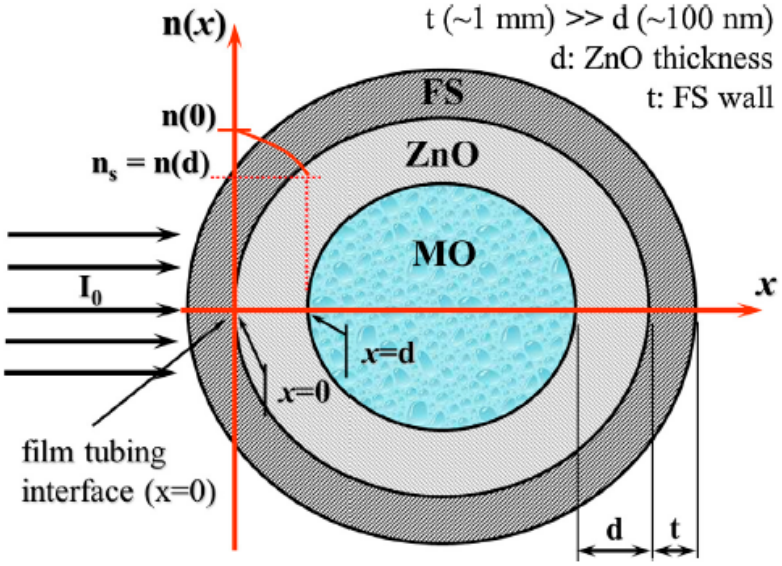

Fig. 1. Transversal cross section of silica tubing illustrating the system used for the evaluation of photocatalytic activity of the ZnO films. The irradiation of the tubing-film array was external. It also presents the one dimensional coordinate used to calculate the photo-generated carrier density $n(x)$ inside the ZnO film; its origin coincide with the interface tubing-film.

It is shown the internal tubing wall coated by the ZnO photocatalyst of thickness d, MO solution inside the tubing and external irradiation Io from the left. The absorbance spectrum of the irradiated solution was recorded, in the range of 220–650 nm, using a fused silica cell of 1 cm side, and distilled water as a blank. In addition the irradiance at 365 nm of the UV-A lamp was measured, before and after sample irradiation by means of a radiometer (UVP model UVX). Table 2 presents the main conditions of this examination. The initial set of experiments determined that a solution concentration of 0.031 mmol L^{-1} and 3 h of exposition gave convenient conditions to compare the photocatalytic activity of different ZnO coated tubular reactors, since up to 90–95% of degradation was obtained. Uncoated tubing was additionally used as blank.

The photocatalytic activity of several films were evaluated as a function of MO concentration in the range of 3.1×10^{-6} to 1.5×10^{-4} mol dm^{-3}; irradiation time from 1 to 18 h; and irradiation intensity in the range of 0.7–3.7 mW cm^{-2}.

Calculations of carrier density distribution, surface concentration of charge carriers and reaction rate

To explain the influence of the films thickness on the photocatalytic activity, in this tubular configuration with external irradiation; a one-dimensional model was proposed to calculate the spatial distribution of the carrier density n(x) and the films' surface charge carrier concentration. This one dimensional approximation is justified by the very small thickness (hundreds of nm) of the films compared to the internal radii of the tubing (several mm). One dimensional analytic result was compared with numerical solutions of the cylindrical differential equation with axial and azimuthal symmetry, given an exact concordance for films of less than 200 nm of thickness. Fig. 1 illustrates the one dimensional system used to calculate the photo-generated carrier density n(x) inside the ZnO film; the origin of this coordinate coincide with the interface tubing-film, it is also depicted the carrier density distribution n(x).

Table 1
Principal synthesis conditions, thickness and grain size of ZnO films deposited in this work.

Parameters	Sample									
	107	108	109	105	101	102	103	100	104	106
Furnace temperature [°C]	250	300	350	400	450	450	450	500	500	500
Deposition time [min]	45	45	40	30	10	20	30	7.5	20	40
Solution flow rate [mL min^{-1}]	0.9	0.8	0.9	0.9	1.0	1.0	0.9	1.4	0.9	0.9
Thickness [nm]	77	78	92	92	51	94	194	29	89	86
Grainsize [nm]	–	–	–	142 ± 18	76 ± 9	228 ± 27	383 ± 44	–	274 ± 50	–

Quasi-steady-state carrier density distribution was calculated by solving the one dimensional stationary continuity equation [34]:

$$D\frac{d^2n(x)}{dx^2} - \frac{n(x)}{\tau} + G(x) = 0 \qquad (1)$$

where, n(x) is the carrier concentration (either electrons or holes) at a distance x from the film-tubing interface; D is the diffusion coefficient of the charge carriers; τ is their lifetime; and G(x) is the volumetric carrier photogeneration rate at x. Origin of spatial coordinate correspond to the film-tubing interface.

Since, UV-A irradiation was external to the tubing (photons incident on the film from the opposite side of its surface), the volumetric carrier photogeneration rate G(x) ($cm^{-3}\,s^{-1}$) at a distance x from the interface film-tubing, can be expressed as

$$G(x) = X \cdot \alpha(\lambda) \cdot F_{ph} \cdot e^{-\alpha(\lambda)\cdot x} \qquad (2)$$

where, X is the quantum efficiency to create an electron–hole (e–h) pair per absorbed photon; α(λ) is the absorption coefficient of the ZnO film, at the wavelength λ; and F_{ph} is the incident photon flux of wavelength λ (photons $cm^{-2}\,s^{-1}$).

Boundary conditions for this quasi-steady approach are:

$$D \cdot \left.\frac{dn(x)}{dx}\right|_{x=d} = -s \cdot n(d) \qquad (3)$$

$$D \cdot \left.\frac{dn(x)}{dx}\right|_{x=0} = 0 \qquad (4)$$

where, s is the coefficient of surface recombination; n(d) is the carrier concentration at the surface of the film (x = d). The other boundary condition considers no recombination at the film-tubing interface (x = 0).

Then, the solution of the continuity equation (1) in the quasisteady- state approach, with boundary conditions (3) and (4), and the carrier photogeneration function (2), yields the spatial distribution of carrier density n(x) and the surface carrier concentration [n_s]:

$$n(x) = C_1 \cdot e^{x/L} + C_2 \cdot e^{-(x/L)} + \frac{A}{\alpha \cdot L} e^{-\alpha \cdot x} \tag{5}$$

and

$$[n_s] = n(d) \tag{6}$$

with

$$C_1 = A \cdot [1 - \sigma], \quad C_2 = -A \cdot \sigma, \tag{7}$$

and $L = (D \cdot \tau)^{1/2}$where

$$A = \frac{X \cdot \alpha^2 \cdot F_{ph} \cdot L}{D \cdot (L^{-2} - \alpha^2)} \tag{8}$$

$$\sigma = \left[\frac{e^{d/L}(1 + \xi) - e^{-\alpha \cdot d}(1 - (\xi/(\alpha \cdot L)))}{e^{d/L}(1 + \xi) - e^{-(d/L)}(1 - \xi)} \right] \tag{9}$$

$$\xi = \frac{s \cdot L}{D} \tag{10}$$

https://cimav.repositorioinstitucional.mx/jspui/

Table 2
Conditions for the photocatalytic evaluation of ZnO film covered tubing.

Sample	Irradiation time (h)	Initial intensity (mW/cm^2)	Final intensity (mW/cm^2)	Volume of solution (mL)	Solution concentration ($mol\,L^{-1}$) 10^{-5}
100	3	7.8	7.0	2.0	3.0
101	3	7.8	7.0	2.0	3.0
102	3	8.2	6.8	2.0	3.0
103	3	8.2	7.2	2.0	3.0
104	3	8.2	6.8	2.0	3.0
105	3	6.8	6.8	2.0	3.0
106	3	8.2	7.2	2.0	3.0
107	3	4.0	3.8	1.8	3.0
108	3	4.0	3.8	1.8	3.0
109	3	6.8	6.7	2.0	3.0
102	3	8.0	7.2	1.8	15.2
102	3	7.6	7.0	1.8	12.2
102	3	7.5	7.0	1.8	9.1
102	3	7.4	7.0	1.8	6.1
102	3	3.8	3.5	1.6	3.0
102	3	4.0	3.7	1.5	1.5
102	3	3.7	3.7	1.5	0.30
102	1	3.8	3.8	1.5	3.0
102	2	3.8	3.7	1.5	3.0
102	3	3.7	3.5	1.5	3.0
102	4	3.4	3.5	1.5	3.0
102	18	3.4	3.4	1.5	3.0

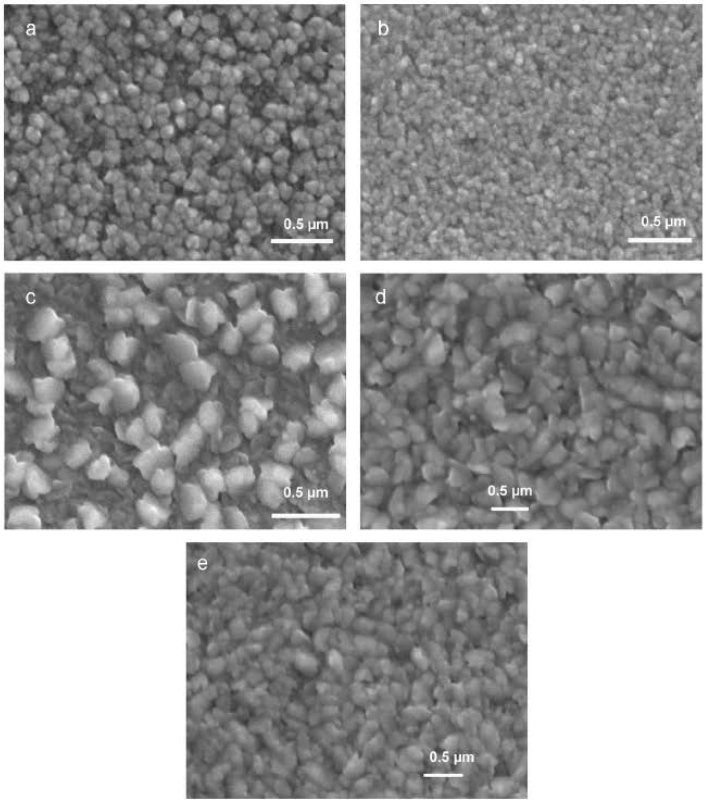

Fig. 2. Secondary electron micrographs of ZnO film coated tubing synthesized at different temperatures and deposition time. (a) sample 105 at 400 °C with 92 nm of thickness; (b) sample 101 at 450 °C with 51 nm of thickness; (c) sample 102 at 450 °C with 92 nm of thickness; (d) sample 103 at 450 °C with 194 nm of thickness; and (e) sample 104 at 500 °C with 89 nm of thickness.

The reaction rate can be related to the surface carrier concentration [n_s] by

$$\frac{dC}{dt} = k \cdot [C] \cdot [n_s] \qquad (11)$$

where, k is the rate constant of adsorbed molecules, and [C] is the concentration of adsorbed molecules. Then the photocatalytic activity of the film will be proportional to the surface carrier concentration [n_s], considering that k and [C] are independent of [ns].

Results and discussion

Microstructural characterization: Fig. 2 shows secondary electron SEM micrographs of the surface morphology of representative ZnO covered silica tubing, to show the influence of deposition temperature and film thickness. Fig. 2(a) shows the morphology of sample 105 deposited at 400 °C, it is shown a tapered microstructure with domed tops, as described in previous works [35,36]; its grains showed uniformly distributed, closely packed and around 142 ± 18 nm of size. Fig. 2(b) shows the surface of sample 101, deposited at 450 °C; the microstructure is similar to sample 105, but composed of smaller grains of around 76 ± 9 nm, as a consequence of the lower thickness (51 nm) of this sample, due to the smaller deposition time (10 min). Fig. 2(c) shows the morphology of sample 102, deposited at 450 °C with 92 nm of thickness; the microstructure displays large flake-like grains [36], of around 200–300 nm, covering 60–70% of the sample surface, with its basal plane inclined in relation to the substrate surface. Fig. 2(d) presents the surface of sample 103, deposited at 450 °C with 194 nm of thickness; a microstructure of densely packed flakelike grains that coat the entire surface. Fig. 2(e) shows the surface morphology of sample 104, deposited at 500 °C with 89 nm of thickness; the microstructure presents a mixture of large tapered and

flake-like grains. It was found differences of grain morphology and grain size between samples deposited at different temperatures and deposition time. For different synthesis temperature and constant thickness, grain size increases due to a favored reaction kinetics. On the other hand, for different film thickness (variable deposition time) and fixed temperature, grain size also increase due to an increase in growth rate (see Table 1). Similarly, grain morphology change from tapered to flake-like as the film thickness increases. It was reported that the photocatalytic activity of the films depend on its grain size, its morphology and its surface area [37,38]. It is known that the increased photocatalytic activity of films synthesized at higher temperatures can be related with the surface morphology, crystal structure and grain size. Grain size and morphology are related to rugosity of the sample surface; higher grain size increase rugosity, some particular grain morphology can also increase surface rugosity, and consequently modify the surface area. It is clear that photocatalytic activity will be enhanced with high surface area, because more adsorption centers can be present. EDS analysis did not show any evidence of contaminants; in addition atomic ratio Zn/O was close to the ideal stoichiometric.

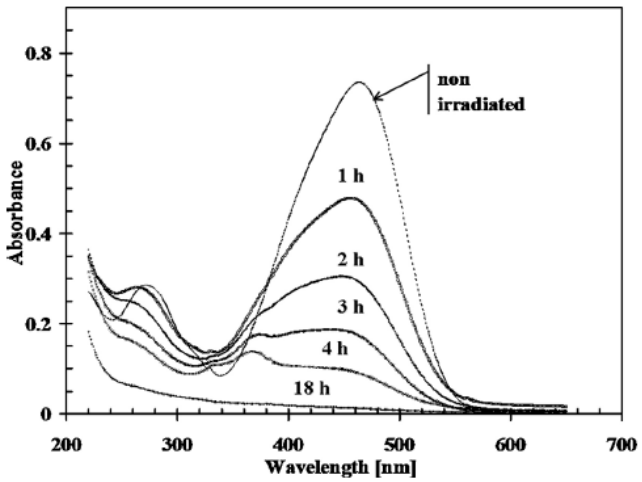

Fig. 3. Absorbance spectra of non-irradiated and irradiated (1–4 h, and 18 h) MO solution (0.031 mM) with sample 102. Conditions were: initial intensity of 8.2 mW cm^{-2}, volume of solution of 2 mL and solution concentration of 3.05×10^{-2} mmol L^{-1}.

Evaluation of photocatalytic activity of ZnO film coated tubing. Influence of MO concentration, irradiation time, and irradiation intensity on the photonic efficiency: The absorption band at 460 nm was used to quantify the photocatalytic decomposition of MO. With the calibration curve of absorbance as a function of MO solution concentration a linear correlation was obtained at low concentration (C < 0.21 mmol L^{-1}). A quantitative correlation between absorbance and solution concentration C was performed by a linear least square fit in this interval, it is found:

ABS=0.0706. [C]

where, ABS is the measured absorbance around 460 nm of the MO solution, and [C] is the MO concentration. This calibration was used to quantify the final concentration of irradiated MO solutions.

No significant discoloration of the MO was observed, neither by photolysis when the solution was placed inside of bare fused silica tubing under long wave UV-A

irradiation, nor in the dark in contact with a ZnO thin films, during 18 and 65 h, respectively.

Fig. 3 shows characteristic absorbance spectra of non irradiated and irradiated (1–4 h) MO solution (0.031 mmol L^{-1}). For this measurement sample 102 was selected as representative of other samples, because it has a medium film's thickness (~94 nm) and grain size (228 nm); this sample was also used to evaluate the influence of the initial concentration of MO solution, irradiation time, and irradiation intensity. It was noticed that the absorbance bands at 270 and 460 nm decrease monotonically with irradiation time and new bands started to form at ~330 and ~365 nm, suggesting the formation of new compounds [39]. It is also plotted in Fig. 3, a test for long period of irradiation (18 h), it is shown that all intrinsic and created bands disappeared, suggesting a complete photodegradation in presence of UV.

The variation of the average photonic efficiency (see Appendix) as a function of the initial concentration of MO solution is presented in Fig. 4. Typical Langmuir–Hinshelwood kinetics can be seen, confirming the heterogeneous character of the system [40].

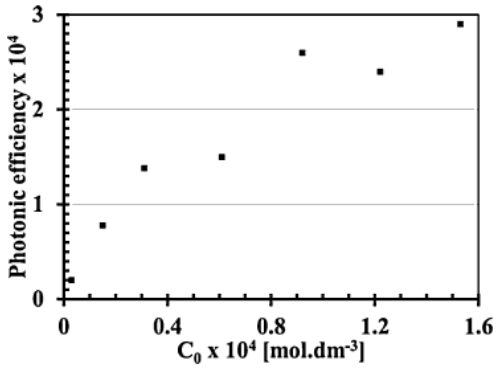

Fig. 4. Average photonic efficiency of ZnO film deposited at 450 °C (sample 102) as a function of the initial concentration of MO solution.

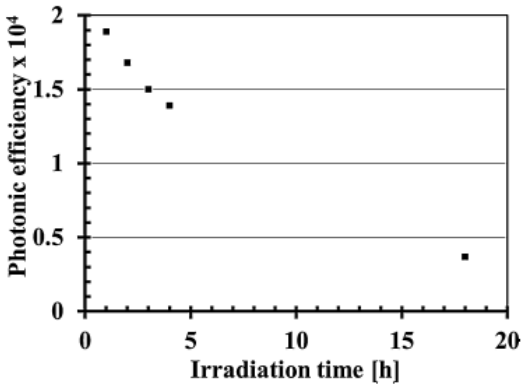

Fig. 5. Variation of the average photonic efficiency of ZnO deposited at 450 °C (sample 102) with irradiation time from 1 to 18 h.

For diluted solutions (C < 0.1 mmol L^{-1}) the reaction is first order, whereas for higher concentrations (C > 0.2 mmol L^{-1}), the reaction rate is maximum with zero order.

Fig. 5 presents the variation of the average photonic efficiency with the irradiation time. The decrease of $<n_{ph}>$, from ~1.9×10^{-4} to ~3.5×10^{-5} is shown, as the irradiation time increases, from 1 to 18 h. This behavior is consistent with the diminution of solution concentration as the irradiation time increase; on the contrary, the average reaction rate also decreases (see Eq. (11)) due to the loss of film's thickness by the dissolution effect.

Fig. 6 shows the average photonic efficiency as a function of irradiation intensity. For low intensity (Io < 1.5 mW cm^{-2}), the photonic efficiency slightly decreases, from 2.9×10^{-4} to 2.1×10^{-4}, as the irradiation intensity increase from ~0.65 to 1 mW cm^{-2}. Then, if the intensity increases further, in the range of ~1.5 to 3.7 mW cm^{-2}, $<n_{ph}>$ remained almost constant, around 1.0×10^{-4}. This performance was expected due to the increase of the quantum yield as the irradiation intensity decreased, it was attributed

to the effect of incident intensity on the relative rates of recombination of electron–hole pairs, similar to the behavior reported for TiO_2 [41,42].

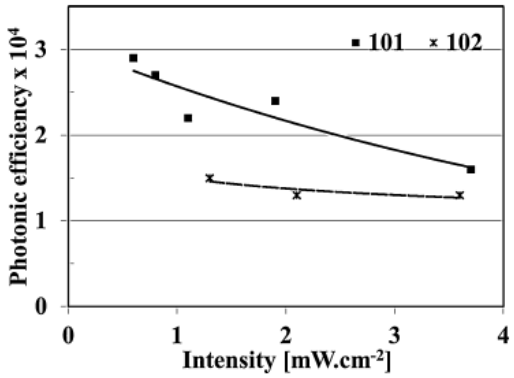

Fig. 6. Average photonic efficiency of ZnO films as a function of irradiation intensity. (■) Film 101; and (*) film 102. The samples were irradiated for 3 h and the solution concentration was 3.05×10^{-2} mmol L^{-1}.

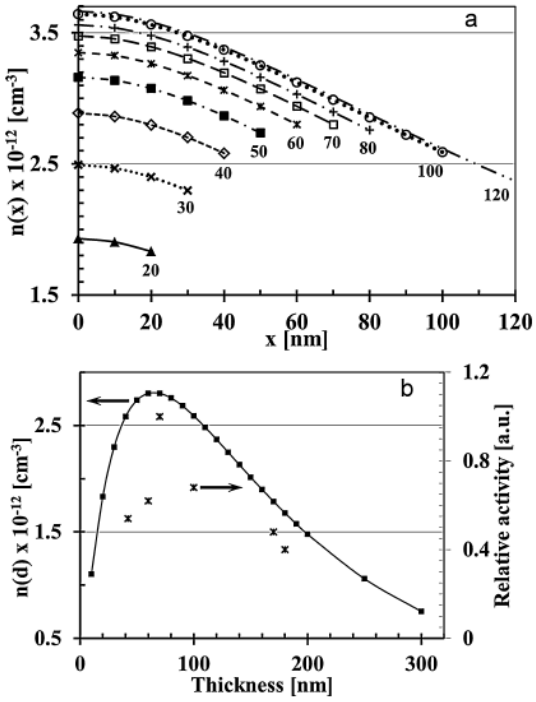

Fig. 7. (a) Photogenerated carrier concentration $n(x)$ distribution calculated for films from 20 to 120 nm of thickness. (b) Surface carrier concentration [n_s], as a function of film thickness. Points (*) are relative experimental activity of different ZnO films with particular thickness.

Correlation of calculated carrier concentration and experimental relative activity: Photogenerated carrier concentration n(x) and surface carrier concentration n_s were calculated following the one dimensional model of Section 3; the parameters used were: α (365 nm) ~2.0×10^5 cm−1 [43]; τ ~ 1.0×10^{-8} s; D ~ 2.0×10^{-2} cm^2 s^{-1}; and s ~ 1.0×10^3 cm s^{-1} [44]. With these parameters, the diffusion length ($L = \tau^{1/2} \cdot D^{1/2}$) of the photocarriers was on the order of 140 nm. Fig. 7a shows the distribution of the photogenerated carrier concentration n(x) calculated for several films of different thickness. In this graph, the origin (x = 0) correspond to the film-substrate interface, while the last right point of each curve, correlate to the charge carrier concentration at the film's surface. Surface carrier concentration, n(d), was plotted as a function of film's thickness in Fig. 7b. It is shown that ns increases as the films' thickness (d) approaches to the diffusion length (L) of the carriers. With a further increase of the film thickness, n_s decays. Consequently, there is an optimum thickness for which the surface carrier density is maxima. Then, as shown in Eq. (11), the photocatalytic activity should be also maxima, since it is proportional to the surface carrier concentration. A qualitative comparison of ns with experimental relative activity of several samples of different thickness will be discussed below.

The relative activity of several films was obtained considering the concentration difference of MO before and after irradiation. Corrections to this value have been made to consider small variation of irradiation intensity and MO solution volume, finally the corrected value was normalized to the highest activity. The most important parameter that influences film activity was the film thickness. Fig. 7b presents the relative activity of

different ZnO films as a function of their thickness, superposed to the surface carrier concentration n(d). A sharp initial increase of the relative activity was found as the film's thickness increases up to 70 nm. With a further increase of the film thickness the activity decreases; this tendency was the same independent of the deposition temperature of the film. It can be qualitatively explained by the dependence of the surface carrier density on the films' thickness and by the ZnO absorbency.

In the case of external irradiation of film coated tubing, the electron–hole (e–h) pairs are photogenerated more intensely close to the interface film-tubing (x = 0); these carriers have to migrate to the surface of the film (x = d) in order to contribute to the photocatalytic process. Thus, the film thickness constitutes a crucial parameter that determines the photocatalytic activity of the film. Consequently, relative activity should increase as a function of film thickness, only in the case where the film thickness (d) is small or approximately to the diffusion length (L) of the photogenerated species. In this circumstance, almost all of the e–h pair photogenerated in the volume of the film were able to diffuse to the film surface, contributing to photocatalytic reaction [34]. Therefore, in this thickness interval ($d \leq L$), as the photogenerated carriers increase with film thickness, the surface carriers also increase, contributing to the photocatalytic reaction, and increasing the activity of the film. However, for a further increase of thickness ($d > L$), there are more photogenerated e–h in the film's volume, but not all of them are able to diffuse to the surface; as a consequence, there are less surface carriers that contributed to the photocatalytic reaction, and the activity declined. This explanation is consistent with results of the one-dimensional model developed in Section 3.

Conclusions

A one-dimensional model of the surface carrier concentration, for the case of external irradiation, was employed to explain qualitatively the variation of the reaction rate of the MO discoloration as a function of the film thickness. In the case of external irradiation of the tubing, an optimum thickness of around 60–70 nm was predicted, for which the surface carrier concentration, consequently the reaction rate, was maximum. Films thinner and thicker than 60–70 nm, have lower reaction rate.

Average photonic efficiency decreased, from 2.9×10^{-4} to 2.1×10^{-4}, as the irradiation intensity increased from ~0.65 to 1 mW cm^{-2}. This performance was expected due to the decreases of the quantum yield as the irradiation intensity increases, attributed to the effect of incident intensity on the relative rates of recombination of electron–hole pairs.

Acknowledgments

The authors would like to thank E. Torres, K. Campos, O Solis, C. Leyva, C. Ornelas, S. Miranda for experimental assistance. This work was partially supported by a grant from CONACYT project N◦ 106655.

Appendix

Average photonic efficiency

The average photonic efficiency of a photocatalytic process can be defined starting from the definition of photonic efficiency [45] as follows:

$$\eta_{\mathrm{ph}} = \frac{dN/dt}{dN_{\mathrm{ph}}/dt} \qquad (12)$$

where, in the particular case treated in this work, n_{Ph} is the photonic efficiency, dN/dt is the number of MO molecules degraded in the system per unit time (molecules s^{-1}); and dN_{ph}/dt is the number of incident photon on the tubing per unit time (photon s^{-1}), at a given wavelength (365 nm). In general, n_{ph} is a function of time, concentration of MO, light intensity, and wavelength (energy) of the photons.

The average photonic efficiency $\langle n_{ph} \rangle$ has been calculated from the following expression:

$$\langle \eta_{Ph} \rangle = \frac{\int_0^{\Delta t} (dN/dt)dt}{\int_0^{\Delta t} (dN_{ph}/dt)dt} = \frac{\Delta N}{\langle N_{ph} \rangle} \qquad (13)$$

where, ΔN is the total number of degraded MO molecules for the irradiation interval Δt, $\langle N_{ph} \rangle$ is the total number of incident photons (365 nm). ΔN can be calculated from:

$$\Delta N = ([C_0] - [C_f]) \cdot V \qquad (14)$$

where, $[C_0]$ and $[C_f]$ are the initial and final MO concentration, respectively; V is the MO volume. Additionally, $\langle N_{ph} \rangle$ was determined from:

$$\langle N_{ph}(\lambda) \rangle = \frac{I_o(\lambda) \cdot S \cdot \Delta t}{E_\lambda} \qquad (15)$$

where $I_o(\lambda)$ is the irradiance (W cm^{-2}) at λ, S is the effective irradiated surface area (cm^2) of the film, Δt is the irradiation time (s), E_λ is the photon energy (J).

Consequently, the photonic efficiency can be expressed as

$$\langle \eta_{Ph} \rangle = \frac{\Delta N}{\langle N_{ph} \rangle} = \frac{([C_0] - [C_f]) \cdot V \cdot E_\lambda}{I_o(\lambda) \cdot S \cdot \Delta t} \qquad (16)$$

https://cimav.repositorioinstitucional.mx/jspui/

The average photonic efficiency $<n_{ph}>$ will be proportional to the average reaction rate, considering I_o, S and E_λ constants. Considering $<n_{ph}>$, the influence of MO concentration, irradiation time, and irradiation intensity on the activity of ZnO film coated tubing was evaluated.

References

[1] S. Hager, R. Bauer, Chemosphere 38 (1999) 1549–1559.

[2] S. Kaur, V. Singh, J. Hazard. Mater. 141 (2007) 230–236.

[3] W. Jun, Z. Gang, Z. Zhaohong, Z. Xiangdong, Z. Guan, M. Teng, J. Yuefeng, Z. Peng, L. Ying, Dyes Pigm. 75 (2007) 335–343.

[4] W. Lin, W. Yang, S. Jheng, J. Taiwan Inst. Chem. Eng. 43 (2012) 269–274.

[5] K. Hashimoto, H. Irie, A. Fujishima, Jpn. J. Appl. Phys. 44 (2005) 8269–8285.

[6] J. Du, W. Chen, C. Zhang, Y. Liu, C. Zhao, Y. Dai, Chem. Eng. J. 170 (2011) 53–58.

[7] D.F. Ollis, E. Pelizzetti, N. Serpone, Environ. Sci. Technol. 25 (1991) 1522–1529.

[8] M. Miki-Yoshida, V. Collins-Martínez, P. Amézaga-Madrid, A. Aguilar- Elguézabal, Thin Solid Films 419 (2002) 60–64.

[9] N. Kaneva, I. Stambolova, V. Blaskov, Y. Dimitriev, A. Bojinova, C. Dushkin, Surf. Coat. Technol. 207 (2012) 5–10.

[10] B. Dindar, S. Ic¸ li, J. Photochem. Photobiol. A 140 (2001) 263–268.

[11] F. Peng, H. Wang, H. Yu, S. Chen, Mater. Res. Bull. 41 (2006) 2123–2129.

[12] J. Doménech, J. Peral, J. Sol. Energy 41 (1998) 55–59.

[13] L. Selva, G.R. Rajarajeswari, R. Selvin, V. Sadasivam, B. Sivasankar, K. Rengaraj, J. Sol. Energy 73 (2002) 281–285.

[14] S.K. Pardeshi, A.B. Patil, Sol. Energy 82 (2008) 700–705.

[15] J. Doménech, A. Prieto, J. Phys. Chem. B 90 (1986) 1123–1126.

[16] P. Spathis, I. Poulios, Corros. Sci. 37 (1995) 673–680.

[17] A. Sharma, P. Rao, R.P. Mathur, S.C. Ameta, J. Photochem. Photobiol. A 86 (1995) 197–200.

[18] L.M. Saragiotto, H.J. Alves, O.A. Andreo, C.M. Macedo, Dyes Pigm. 76 (2008) 525–529.

[19] M. Toyoda, Y. Nanbu, Y. Nakazawa, M. Hirano, M. Inagaki, Appl. Catal. B 49 (2004) 227–232.

[20] J. Kry´ sa, P. Novotná, ˇS. Kment, A. Mills, J. Photochem. Photobiol. A 222 (2011) 81–86.

[21] P. Zhang, J. Tian, R. Xu, G. Ma, Appl. Surf. Sci. 266 (2013) 141–147.

[22] A. Kulkarni, J. Lee, J. Nam, T. Kim, Sens. Actuat. B 150 (2010) 154–159.

[23] N.J. Peilland, M.R. Hoffmann, Environ. Sci. Technol. 30 (1996) 2806–2812.

[24] D. Wang, X. Li, J. Chen, X. Tao, Chem. Eng. J. 198/199 (2012) 547–554.

[25] Y. Kikuchi, K. Sunada, T. Iyoda, K. Hashimoto, A. Fujishima, J. Photochem. Photobiol. A 106 (1997) 51–56.

[26] L. Xu, X. Li, Y. Chen, F. Xu, Appl. Surf. Sci. 257 (2011) 4031–4037.

[27] L. Xu, L. Shi, X. Li, Appl. Surf. Sci. 255 (2008) 3230–3234.

[28] C. Ho, S.B. Lee, J.H. Boo, Thin Solid Films 475 (2005) 183–188.

[29] M. Miki-Yoshida, W. Antúnez-Flores, K. Gomez-Fierro, L. Villa-Pando, R.

Silveyra-Morales, P. Sánchez-Santiago, R. Martínez-Sánchez, M. José-Yacamán, Surf. Coat. Technol. 200 (2006) 4111–4116.

[30] M.F. Brunilla, M.V. Diamanti, M.P. Pedeferri, F. Di Fonzo, C.S. Casari, A. Li Bassi, Thin Solid Films 515 (2007) 6309–6313.

[31] P. Amézaga-Madrid, W. Antúnez-Flores, J.E. Ledezma-Sillas, J.G. Murillo-Ramírez, O. Solís-Canto, O.E. Vega-Becerra, R. Martínez-Sánchez, M. Miki- Yoshida, J. Alloys Compd. 509S (2011) S490–S495.

[32] W. Nam, J. Kim, G. Han, Chemosphere 47 (2002) 1019–1024.

[33] N. Guettaï, H. Ait Amar, Desalination 185 (2005) 427–437.

[34] A. Emeline, V.K. Ryabchuck, N. Serpone, J. Phys. Chem. B 103 (1999) 1316-1324.

[35] F. Paraguay D, W. Estrada L, D.R. Acosta N, E. Andrade, M. Miki-Yoshida, Thin Solid Films 350 (1999) 192–202.

[36] F. Paraguay D, J. Morales, W. Estrada, L.E. Andrade, M. Miki-Yoshida, Thin Solid Films 366 (2000) 16–27.

[37] A. López, D. Acosta, A.I. Martínez, J. Santiago, Powder Technol. 202 (2010) 111–117.

[38] D.A.H. Hanaor, G. Triani, C.C. Sorrell, Surf. Coat. Technol. 205 (12) (2011) 3658–3664.

[39] S. Al-Qaradawi, S.R. Salman, J. Photochem. Photobiol. A 148 (2002) 161–168.

[40] J.M. Herrmann, Catal. Today 53 (1) (1999) 115–129.

[41] M.A. Aguado, M.A. Anderson, C.G. Hill, J. Mol. Catal. A: Chem. 89 (1994) 165.

[42] A. Fujishima, T.N. Rao, D.A. Tryk, J. Photochem. Photobiol. C 1 (2000) 1–21.

https://cimav.repositorioinstitucional.mx/jspui/

[43] J.F. Ruth, R.M. Kolbas, A.K. Sharma, S. Oktyabrsky, J. Narayan, J. Appl. Phys. 85 (1999) 7884–7887.

[44] O. Lopatiuk, L. Chernyak, A. Osinsky, J.Q. Xie, P.P. Chow, Appl. Phys. Lett. 87 (2005) 162103–162105.

[45] A. Emeline, A. Salinaro, N.N. Serpone, J. Phys. Chem. B 104 (2000) 11202–11210.